Available online at www.sciencedirect.com
SCIENCE DIRECT®
Chemical Physics Letters 383 (2004) 332–342
CHEMICAL PHYSICS LETTERS
www.elsevier.com/locate/cplett

Analysis of the paramagnetic spin–orbit transmission mechanism for NMR spin–spin coupling constants using the paramagnetic spin–orbit density distribution

Jürgen Gräfenstein, Dieter Cremer *

Department of Theoretical Chemistry, Göteborg University, Reutersgatan 2, S-41320 Göteborg, Sweden

Received 2 September 2003; in final form 3 October 2003
Published online: 4 December 2003

Abstract

For the analysis of the paramagnetic spin orbit (PSO) term of the NMR spin–spin coupling constant (SSCC), ring current density and PSO density distribution are derived and used to explain magnitude and sign of the isotropic PSO term. Decomposition of the PSO components into orbital contributions helps to identify those orbital pairs (occupied, virtual) dominating the PSO term. The induction of strong ring currents requires low excitation energies and complementing nodal properties of zeroth and first order orbitals. The PSO components for a typical triple, double, and single CC bond are explained.

1. Introduction

Nuclear magnetic resonance (NMR) spectroscopy is one of the most important tools to investigate molecular structure and molecular conformation [1]. The NMR chemical shifts of a molecule probe the electronic structure in the vicinity of the nuclei while the indirect NMR spin–spin coupling constants (SSCCs) provide valuable insight into the bonding situation of a molecule [1–3]. During the last five decades a wealth of NMR data has been collected and many relationships between the NMR parameters of a molecule and others of its properties have been derived [1–3]. Nevertheless, there is still a lack of understanding concerning the spin–spin coupling mechanism between two nuclei. According to the classic theory of Ramsey [4], there are four different terms, the diamagnetic spin–orbit (DSO) term, the paramagnetic spin–orbit (PSO) term, the Fermi contact (FC) term and the spin–dipole (SD) term, which add to the indirect isotropic SSCC. Each of these terms probes the electron density of a molecule in a different way. DSO and PSO term arise from the orbital currents induced by the magnetic fields of the nuclei, the FC term is mediated by the spin polarization of the contact density at the nuclei while the SD term results from the spin polarization caused by the magnetic dipole field of the nuclear moment. Accordingly, the FC term depends preferentially on the σ-electrons of a molecule because only those possess a substantial density value at the contact surface of the nucleus. The DSO term is large at positions of high density, but otherwise its magnitude is mostly smaller than that of the PSO term. The latter as well as the SD term are sensitive to the presence of π-electrons.

Considering the normally small magnitude of the DSO term, one can simplify these observations by stating that the FC term probes the σ-electronic structure of a molecule while the non-contact (NC) terms probe its π-electronic structure. This could be used to determine via the SSCC and its four Ramsey terms the π-bond character of a bond. For example, in the case of a C–C single bond (ethane), C=C double bond (ethylene) and C≡C triple bond (acetylene), the magnitude of the NC term increases from 1.5 to 23.6 SI units with a minimum of −8.4 SI units for the CC double bond according to SSCC calculations carried out in this work

* Corresponding author. Fax: +46-31-772-2778.
E-mail address: dieter.cremer@theoc.gu.se (D. Cremer).

0009-2614/$ - see front matter © 2003 Elsevier B.V. All rights reserved.
doi:10.1016/j.cplett.2003.10.147

(Table 1). Since the total SSCC compare reasonably with the experimental ^1J(CC) values [5] (vibrational corrections of −10.0–0.9 Hz calculated for ^1J(CC) of acetylene and ethylene have to be added [6]), it is justified to consider also the calculated Ramsey terms of these SSCCs as reasonable. Clearly, there is a relationship between the magnitude of the NC terms and the π-character of the CC bond, which could be exploited to determine the π-character of conjugated, hyperconjugated, homoconjugated or strained CC bonds, thus providing a valuable asset to the description of bonding via measurement of SSCCs. However, two obstacles hinder the direct use of a relationship between the π-character of a bond and the magnitude of the NC terms of the corresponding one-bond SSCC.

1. The SSCC is measured as the sum of the four Ramsey terms. However, the Ramsey terms of the SSCC are not observable quantities.
2. The NC terms are negative for typical C=C double bonds, but positive for typical C≡C triple bonds (Table 1). As long as this is not understood it is difficult to set up a relationship between the π-character of a bond and the value of the NC term of the corresponding one-bond SSCC.

There are well-known relationships between the magnitude of the FC term of a SSCC and the s-character of a bond [7,8]. For example, it is known that the SSCC ^1J(CH) is dominated by the FC term and that both FC term and ^1J(CH) are related to the s-character of the CH bond orbital by the Muller–Pritchard equation [9]. If all ^1J(CH) values for a particular CC bond are known, it is possible to determine via the sum rule for hybrid orbitals [10] the s-character of the hybrid orbitals forming the CC bond. This provides the basis for predicting the FC part of the SSCC ^1J(CC) using for example the Frei–Bernstein equation [11]. The difference between the experimental SSCC ^1J(CC) and the predicted ^{1}FC(CC) value provides a measure for the π-character of the CC bond. This approach can be improved in several ways by determining the s-character of the substituent bonds either via other measured bond properties or by calculating it directly employing quantum chemical methods. In this way, one can get an experimentally-based estimate of the NC term of the SSCC ^1J(CC).

Hence, it remains to clarify trends in the values of the contact term in dependence of the π-character of the bond. We have recently started a research program to decode the spin–spin coupling mechanism in terms of orbital contributions, spin densities and orbital currents. The steps of this program involved: (a) the derivation of a Coupled Perturbed Density Functional (CP-DFT) method to calculate SSCCs is an economical but reliable way [12]; (b) generation of J-hypersurfaces (generalized Karplus relationships) to study the influence of geometrical changes on the SSCC in a systematic way [13]; (c) decoding of time-averaged SSCCs with the help of theory [14]; (d) analysis of the spin–spin coupling mechanism in terms of orbital contributions to the individual Ramsey terms [15]; (e) identification of different coupling paths in a molecule for one particular SSCC (multipath coupling) [16]; (f) description of the FC coupling mechanism with the help of first order molecular orbitals and the FC spin density distribution [17]. The present research report connects directly to the latter work, in which we could show how the FC spin density distribution determines sign and magnitude of a particular orbital term and how certain orbital terms such as bond orbital or lone pair orbital contribution dominate the magnitude of the FC term [17]. In this work, we focus on the PSO term as the most important of the NC terms. We will introduce the PSO density distribution and show how different orbital currents influence sign and magnitude of the PSO part of the SSCC.

The results of this work will be presented in the following way. We will first derive the tools to analyze the PSO term (Section 2). Then, in Section 3 we will demonstrate the usefulness of these tools by explaining the different PSO contributions found for the ^1J(CC) value of a CC double and a CC triple bond. These explanations will be the basis for future work, which focuses on the use of SSCCs as sensitive antennas for the description of chemical bonding (Section 4).

Table 1
The four terms of the isotropic SSCC ^1K(CC) for C_2H_2, C_2H_4 and C_2H_6[a]

Molecule	DSO	PSO	FC	SD	NC	^1K(CC)	^1J(CC)	^1J(exp)[b]
C_2H_2	0.11	9.07	221.52	14.40	23.58	245.09	186.02[c]	169.7
C_2H_4	0.11	−13.12	87.12	4.59	−8.42	78.70	59.73[d]	67.5
C_2H_6	0.17	−0.03	33.13	1.37	1.51	34.65	26.30	34.5

[a] Calculations were carried out at CP-DFT/BPW91/(11s, 7p, 2d/6s, 2p)[7s, 6p, 2d/4s, 2p] using experimental geometries [23,24]. For ethane, the geometrical parameters $r_{CC} = 1.526$ Å, $r_{CH} = 1.088$ Å, $\alpha_{HCH} = 107.4°$ are used taken from E. Hirota, K. Matsumara, M. Imachi, M. Fujio and Y. Tsuno, J. Chem. Phys. 66 (1977) 2660. The CC bonds are oriented along the z axis, the H atoms in C_2H_4 are in the xz plane. Values of the reduced SSCC ^1K(CC) in SI units (10^{19} kg m^{-2} s^{-2} A^{-2}) and of the SSCC ^1J(CC) in Hz.

[b] Experimental values from [5].

[c] 176.0 Hz when vibrational corrections from [6] are added.

[d] 60.6 Hz when vibrational corrections from [6] are added.

2. Derivation of the PSO density distribution

As the present work is concerned with electronic processes connected with spin–spin coupling, we will use the reduced SSCCs K rather than the full SSCCs J so as to make the discussion independent of the gyromagnetic ratios of the nuclei involved.

Ramsey [4] established the microscopic theory of SSCC by employing second-order perturbation theory with respect to the magnetic moments of the coupling nuclei. This derivation can be understood in the way that one of the nuclei (called *perturbing nucleus* in the following) perturbs by its magnetic moment the electron system, which in turn gives rise to a magnetic field at the location of the second (*responding*) nucleus. Within CP-DFT, the SSCC is represented as sum of the four Ramsey terms given by Eqs. (1)–(4) [4,12]

$$K_{\mathrm{AB}}^{\mathrm{DSO}} = \frac{2}{3}\sum_{k}^{\mathrm{occ}} \left\langle \phi_k^{(0)} | \mathrm{Tr}\, \underline{\underline{h}}_{\mathrm{AB}}^{\mathrm{DSO}} | \phi_k^{(0)} \right\rangle, \tag{1}$$

$$K_{\mathrm{AB}}^{\mathrm{PSO}} = -\frac{4}{3}\sum_{k}^{\mathrm{occ}} \left\langle \phi_k^{(0)} | \mathbf{h}_{\mathrm{A}}^{\mathrm{PSO}} | \vec{\phi}_k^{(\mathrm{B}),\mathrm{PSO}} \right\rangle, \tag{2}$$

$$K_{\mathrm{AB}}^{\mathrm{FC}} = \frac{2}{3}\sum_{k\sigma}^{\mathrm{occ}} \left\langle \psi_{k\sigma}^{(0)} | \mathbf{h}_{\mathrm{A}}^{\mathrm{FC}} | \vec{\psi}_{k\sigma}^{(\mathrm{B}),\mathrm{FC}} \right\rangle, \tag{3}$$

$$K_{\mathrm{AB}}^{\mathrm{SD}} = -\frac{2}{3}\sum_{k\sigma}^{\mathrm{occ}} \left\langle \psi_{k\sigma}^{(0)} | \mathbf{h}_{\mathrm{A}}^{\mathrm{SD}} | \vec{\psi}_{k\sigma}^{(\mathrm{B}),\mathrm{SD}} \right\rangle, \tag{4}$$

where the DSO, PSO, FC and SD operators are defined by Eqs. (5)–(8)

$$\underline{\underline{h}}_{\mathrm{AB}}^{\mathrm{DSO}} = \left\{ \frac{1}{m}\left(\frac{4\pi\varepsilon_0\hbar^2}{e^3}\right)^2 \right\} \alpha^4 \left(\frac{\mathbf{r}_{\mathrm{A}}}{r_{\mathrm{A}}^3}\cdot\frac{\mathbf{r}_{\mathrm{B}}}{r_{\mathrm{B}}^3}\underline{\underline{I}} - \frac{\mathbf{r}_{\mathrm{A}}}{r_{\mathrm{A}}^3}\circ\frac{\mathbf{r}_{\mathrm{B}}}{r_{\mathrm{B}}^3} \right), \tag{5}$$

$$\mathbf{h}_{\mathrm{A}}^{\mathrm{PSO}} = \left\{ \frac{4\pi\varepsilon_0\hbar^3}{e^3 m} \right\} \alpha^2 \frac{\mathbf{r}_{\mathrm{A}}}{r_{\mathrm{A}}^3} \times \nabla, \tag{6}$$

$$\mathbf{h}_{\mathrm{A}}^{\mathrm{FC}} = \left\{ \frac{4\pi\varepsilon_0\hbar^3}{e^3 m} \right\} \frac{8\pi}{3} \alpha^2 \delta(\mathbf{r}_{\mathrm{A}})\mathbf{s}, \tag{7}$$

$$\mathbf{h}_{\mathrm{A}}^{\mathrm{SD}} = \left\{ \frac{4\pi\varepsilon_0\hbar^3}{e^3 m} \right\} \alpha^2 \left[3\frac{(\mathbf{s}\cdot\mathbf{r}_{\mathrm{A}})\mathbf{r}_{\mathrm{A}}}{r_{\mathrm{A}}^5} - \frac{\mathbf{s}}{r_{\mathrm{A}}^3} \right]. \tag{8}$$

The position of nucleus N (A or B) is given by vector $\mathbf{R}_{\mathrm{N}}$, $\mathbf{r}_{\mathrm{N}} = \mathbf{r} - \mathbf{R}_{\mathrm{N}}$ gives the distance between electron and nucleus, ε_0 is the dielectric constant of the vacuum, α is Sommerfeld's fine structure constant, $\underline{\underline{I}}$ is the unit tensor and $\mathbf{s}$ is the electron spin in units of $\hbar$. The prefactors enclosed in braces in Eqs. (5)–(8) become equal to one in atomic units. Note that $\mathbf{h}_{\mathrm{A}}^{\mathrm{FC}}$ and $\mathbf{h}_{\mathrm{A}}^{\mathrm{SD}}$ are 2×2 matrices with respect to the electron spin variables. The DSO and the PSO part of the SSCC can be expressed in terms of spin-free orbitals ϕ_k while the FC and the SD part are given in terms of spin-dependent orbitals ψ_k. Zeroth-order orbitals are denoted by superscript (0) while superscript (B) denotes first-order orbitals resulting from the perturbing nucleus B. The indices of the occupied orbitals will be $k, l, \ldots$, those of the virtual orbitals $a, b, \ldots$. The vectors $\vec{\psi}_k^{(\mathrm{B}),\mathrm{X}}$ and $\vec{\phi}_k^{(\mathrm{B}),\mathrm{X}}$ summarize the three first-order orbitals corresponding to the three components of $\mathbf{h}_{\mathrm{B}}^{\mathrm{X}}$ (X = PSO, FC, SD).

In their general definition, the SSCCs are tensors with respect to the orientations of the perturbing and responding nuclei (see e.g. [4]). The isotropic SSCCs as given by Eqs. (1)–(8) are 1/3 of the trace of the corresponding SSCC tensors. They describe the SSCCs averaged over all orientations of the perturbed nucleus and correspond to the results from NMR measurements in gas phase or solution [1–3]. For the purpose of investigating the electronic mechanism of spin–spin coupling, it is necessary to consider the individual diagonal components of the SSCC tensors, which specify the SSCC for a given orientation of the perturbed nucleus. For the DSO and PSO tensors, the diagonal terms along a given direction $\mathbf{n}$ have the form:

$$K_{\mathrm{AB},\mathbf{nn}}^{\mathrm{DSO}} = 2\sum_{k}^{\mathrm{occ}} \left\langle \phi_k^{(0)} | (\mathbf{n}\underline{\underline{h}}_{\mathrm{AB}}^{\mathrm{DSO}}\mathbf{n}) | \phi_k^{(0)} \right\rangle, \tag{9a}$$

$$K_{\mathrm{A,B},\mathbf{nn}}^{\mathrm{PSO}} = -4\sum_{k}^{\mathrm{occ}} \langle \phi_k^{(0)} | (\mathbf{h}_{\mathrm{A}}^{\mathrm{PSO}}\mathbf{n}) | \underbrace{(\mathbf{n}\vec{\phi}_k^{(\mathrm{B}),\mathrm{PSO}})\rangle}_{=|\phi_{k,\mathbf{n}}^{(\mathrm{B}),\mathrm{PSO}}\rangle}. \tag{9b}$$

The DSO and PSO terms describe the coupling between the nuclei mediated by orbital currents in the system. The perturbing nucleus induces a current density in the electron system, which in turn gives rise to an extra magnetic field. The value and orientation of this field at the responding nucleus favors either a parallel or an antiparallel orientation of the magnetic moments of the perturbing and responding nucleus.

For a given orientation $\mathbf{n}$ of the perturbing nucleus, the DSO and the PSO term can be written as a weighted integral over the electronic current density, where the weighting factor extracts that part of the total current density that forms a ring current around nucleus A, i.e., the current density is re-expanded into ring-current contributions around A

$$K_{\mathrm{AB},\mathbf{nn}}^{\mathrm{X}} = \left\{ \frac{1}{m}\frac{4\varepsilon_0\hbar^2}{e^3} \right\} \alpha^2 \int \mathrm{d}^3 r\, \mathbf{n}\left(\mathbf{j}_{\mathbf{n}}^{(\mathrm{B}),\mathrm{X}}(\mathbf{r}) \times \frac{\mathbf{r}-\mathbf{R}_{\mathrm{A}}}{|\mathbf{r}-\mathbf{R}_{\mathrm{A}}|^3} \right), \tag{10}$$

where now X = PSO, DSO and $\mathbf{j}_{\mathbf{n}}^{(\mathrm{B}),\mathrm{X}}(\mathbf{r})$ are the first-order PSO and DSO currents for a perturbation at nucleus B:

$$\mathbf{j}_{\mathbf{n}}^{(\mathrm{B}),\mathrm{DSO}}(\mathbf{r}) = -\left\{ \frac{1}{m}\frac{4\varepsilon_0\hbar^2}{e^3} \right\} \alpha^2 \varrho^{(0)}(\mathbf{r}) \left(n \times \frac{\mathbf{r}-\mathbf{R}_{\mathrm{B}}}{|\mathbf{r}-\mathbf{R}_{\mathrm{B}}|^3} \right), \tag{11a}$$

$$\mathbf{j}_{\mathbf{n}}^{(\mathrm{B}),\mathrm{PSO}}(\mathbf{r}) = 2\left\{\frac{\hbar}{m}\right\}\sum_{k}^{\mathrm{occ}}\left[\phi_{k,\mathbf{n}}^{(\mathrm{B}),\mathrm{PSO}}(\mathbf{r})\nabla\phi_{k}^{(0)}(\mathbf{r}) - \phi_{k}^{(0)}(\mathbf{r})\nabla\phi_{k,\mathbf{n}}^{(\mathrm{B}),\mathrm{PSO}}(\mathbf{r})\right], \tag{11b}$$

with $\varrho^{(0)}(\mathbf{r}) = 2\sum_{k}^{\mathrm{occ}}|\phi_{k}^{(0)}(\mathbf{r})|^2$ being the zeroth-order electron density.

An unambiguous separation between DSO and PSO term is not possible. The gauge ambiguity of the magnetic vector potential allows to move contributions to the current density between PSO and DSO term. Also, the PSO and the DSO current densities usually do not fulfill the continuity equation one by one but only in their sum. Still, DSO and PSO terms describe different induction mechanisms: the DSO term describes the induction of ring currents by Larmor precession (see Fig. 1a). This effect is present for any orbital. The PSO term, in contrast, describes the modification of existing ring currents by the magnetic moment. This is shown in Fig. 1b: assume that a pair of (complex) orbitals $p_{\pm}$ in an atom is fully occupied (the PSO term is easiest to discuss for complex orbitals; note that $p_{\pm}$ forms a torus in real space, which is schematically indicated in Fig. 1b). The p_{+} and p_{-} electron carry opposite ring currents, which cancel each other exactly. If a magnetic perturbation is applied, the $p_{\pm}$ electrons are influenced in an opposite way. One of the two ring currents is increased, while the other is decreased, which results in a non-vanishing net ring current for the $p_{\pm}$ orbital pair. The PSO mechanism is effective only for orbitals with non-s character around the perturbed nucleus A. For these orbitals, however, it typically outweighs the DSO contribution.

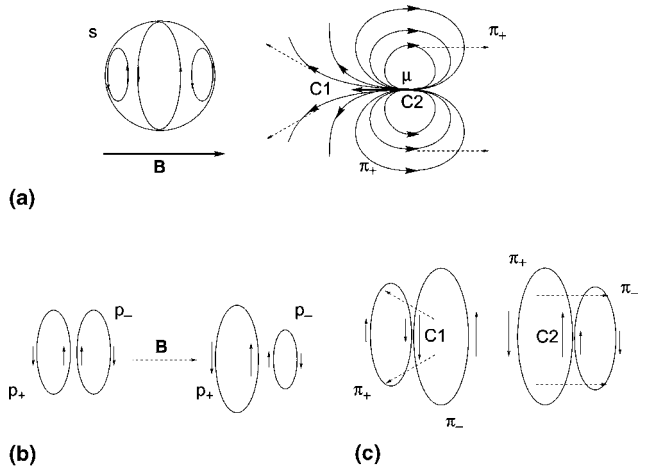

Fig. 1. (a) Induction of diamagnetic currents in an atomic s orbital, (b) induction of paramagnetic ring currents in a pair of atomic $p_{\pm}$ orbitals. (c) The induced ring currents in C_2H_2 for the perturbing nucleus along the C≡C axis. The upper part shows the magnetic dipole field generated by the magnetic moment $\vec{\mu}$ of nucleus C2. For some positions close to C2 and C1, the magnetic field is marked with dashed arrows. In the lower part, the modification of the ring currents by the magnetic dipole field is shown. The dashed arrows for **B** are repeated in the lower part to indicate that **B** points to the right around C2 while it points to he left around Cl. This opposite orientation of **B** around C1 and C2 gives rise to the opposite orientation of the induced ring currents.

The operator $\mathbf{h}_{\mathrm{B}}^{\mathrm{PSO}}$ is essentially the operator for the orbital angular momentum related to $\mathbf{R}_{\mathrm{B}}$, weighted with $|\mathbf{r}-\mathbf{R}_{\mathrm{B}}|^{-3}$. This implies that only occupied and virtual orbitals contribute to the PSO term that have non-s character at B, which is in line with the picture that the PSO mechanism modifies existing orbital currents. Often the PSO mechanism is realized with p orbitals. In this case, for the perturbing moment oriented in z direction, only excitations of the kind $p_{+} \rightarrow p_{+}^{*}$ and $p_{-} \rightarrow p_{-}^{*}$ contribute to the PSO mechanism. If real orbitals rather than complex ones are considered, the corresponding transitions are $p_x \rightarrow p_y^{*}$ and $p_y \rightarrow p_x^{*}$.

The considerations in connection with the PSO and DSO mechanisms can be directly generalized to molecules, where the role of the p orbitals is taken over by π orbitals.

We calculated SSCCs for C_2H_2 and C_2H_4 employing CP-DFT [12] for the BPW91 exchange-correlation functional [18–20] and the (11s,7p,2d/6s,2p)[7s,6p,2d/4s,2p] basis set [21,22] designed for the calculation of magnetic properties. Experimental geometries were used: $r_{\mathrm{CC}} = 1.203$ Å, $r_{\mathrm{CH}} = 1.061$ Å for C_2H_2 [23], $r_{\mathrm{CC}} = 1.339$ Å, $r_{\mathrm{CH}} = 1.088$ Å, $\alpha_{\mathrm{HCH}} = 117.4°$ for C_2H_4 [24].

For the PSO contribution of the SSCC, the diagonal components of the SSCC tensor were calculated individually. Reduced SSCCs K are given in SI units, i.e., 10^{19} kg m^{-2} s^{-2} A^{-2}, while J values are given in Hz where the conversion factor from K(CC) to J(CC) is 0.759.

Utilizing calculated $|\phi_{k}^{(0)}\rangle$ and $|\vec{\phi}_{k}^{(\mathrm{B}),\mathrm{PSO}}\rangle$, we performed a local analysis of the contributions to the PSO term. As revealed by Eq. (10), the PSO term can be represented as a weighted integral over the current density $\mathbf{j}_{\mathbf{n}}^{(\mathrm{B}),\mathrm{PSO}}(\mathbf{r})$. The PSO mechanism will be efficient only if: (i) the perturbing nucleus induces paramagnetic ring currents in the electron system and (ii) these ring currents are effective in generating a magnetic field at the position of the responding nucleus. We studied therefore both the distribution of $\mathbf{j}_{\mathbf{n}}^{(\mathrm{B}),\mathrm{PSO}}(\mathbf{r})$ for given orientations of the perturbing nucleus and the weighted current density, i.e., the integrand in Eq. (10) for X = PSO, for which we coined the term *PSO density distribution*. The current densities are represented as contour plots in a plane perpendicular to a component of the actual current. This representation gives a better account of the current distribution than stream lines or arrows in situations where the current densities vary by several orders of magnitude. Furthermore, stream lines are problematic when the current density is not divergence-free. The PSO densities, which are scalar, are also

represented as contour plots. It should be noted that the plots of the current densities are specific to the perturbing nucleus only, whereas plots of the PSO density are specific for both the perturbing and the responding nucleus.

For the purpose of identifying the main orbital contributions to the PSO term, we used the J-OC-PSP (decomposition of J into Orbital Contributions using Orbital Currents and Partial Spin Polarization) developed recently [15,17]. All SSCC calculations were carried out with the CP-DFT algorithm [12] implemented in the ab initio program package COLOGNE 2003 [25].

3. Results and discussion

First we will discuss results for the PSO term of the SSCC ^1J(CC) of acetylene, then the corresponding results for ethylene. The two CC bonds in these molecules can be considered as the prototypes for all triple or double bonded first row systems. CP-DFT values of the three PSO components, as well as the orbital contributions for the C–C bond orbitals determined with the J-**OC**-PSP analysis [15,17], are summarized in Table 2 where as a reference the corresponding values of the ^1J(CC) constant of ethane are added. Calculated current densities and PSO densities are graphically displayed in form of contour line diagrams in Figs. 2 (acetylene) and 3 (ethylene). For the current density dashed contour lines indicate that the current flows from above the plane into the plane perpendicular through the center of the closed contour lines. For solid contour lines the flow direction is opposite. In all plots discussed in the following, C2 is the perturbing nucleus and Cl the responding one. The bond axis will give the z-direction, the xz-plane will be the molecular plane of ethylene and the y-direction will be the direction of the π-orbitals. The contour line values are given in form of a geometric progression using a multiplication factor of $100^{1/5} = 2.5118864$. In this way, the contour level value of each fifth contour line has increased (decreased) by a factor of 100. For the purpose of simplifying the comparison of the diagrams shown in Figs. 2 and 3, the contour lines with the values 0.1 and 10 are given in bold.

3.1. PSO term for ^1J(CC) of acetylene

Fig. 2a shows a contour plot of the perpendicular current density for C_2H_2 in the yz-plane containing the axis of the molecule with the perturbing nuclear moment along the CC bond direction (z-direction). The diagram reveals that the nucleus induces relatively large ring currents, which are of opposite direction around Cl and C2. If one looks from C2 to Cl, the ring current at Cl is clockwise around the CC axis while that at C2 is counterclockwise oriented. The former is clearly larger than the latter as reflected by the extension of the current densities into space. Fig. 2b shows the corresponding PSO density. One finds that the ring current around Cl makes a positive contribution to the PSO term, the ring current around C2, a negative one. Especially, for small distances from the CC bond, the positive contribution is larger than the negative one. This effect is enlarged by the fact that the PSO_{zz} density of Fig. 2b is rotational symmetric around the z-axis. Integration according to Eq. (10) eventually leads to a value of +63.3 SI units for $^1K_{zz}^{PSO}$ (CC) (see Table 2).

The opposite directions of the paramagnetic ring currents around the two C atoms can be rationalized considering the form of the magnetic dipole field (see Fig. 1c): In the π-space of C2, this field points preferentially in the direction Cl → C2, however in the π-space of C1 in the opposite direction (dashed arrows in Fig. 1c). An orbital analysis of the current density shows that the ring currents are mainly due to excitations from the $\pi_\pm$ orbitals in the corresponding $\pi_\pm^*$ orbitals. This excitation allows for an efficient induction of paramagnetic ring currents for a number of reasons: (i) the zero-order – first-order orbital pairs involving $\pi_\pm$ and $\pi_\pm^*$ overlap strongly thus facilitating excitations (actually, one has to consider the products $\phi_k^{(1)}\nabla\phi_k^{(0)}$ and $\phi_k^{(0)}\nabla\phi_k^{(1)}$ in Eq. (11)); (ii) the excitation energy is relatively low (BPW91/[7s,6p,2d/4s,2p] orbital energies of −0.263 and −0.011 a.u., respectively); (iii) the nodal

Table 2
Diagonal components of the PSO part of the SSCC ^1K(CC) of C_2H_2, C_2H_4 and C_2H_6 and contributions from the C–C bonding orbitals[a]

Orientation	C_2H_2			C_2H_4			C_2H_6	
	Total	σ(C1C2)	π_x(C1C2)	Total	σ(C1C2)	π_y(C1C2)	Total	σ(C1C2)
xx	−18.05	−12.97	0.07	−33.79	−18.01	−7.13	0.98	−1.43
yy	−18.05	−12.97	1.15	−0.15	−1.99	0.05	0.98	−1.43
zz	63.31	0.0	31.65	−5.43	0.00	−0.74	−2.04	0.00
Isotropic	9.07	−8.65	10.96	−13.12	−6.67	−2.61	−0.03	−0.95

[a] Calculations done at CP-DFT/BPW91/(11s,7p,2d/6s,2p)[7s,6p,2d/4s,2p] using experimental geometries [23,24]. Orbital contributions to the PSO terms obtained by a J-**OC**-PSP analysis according to [15,17]. For further details see note in Table 1.

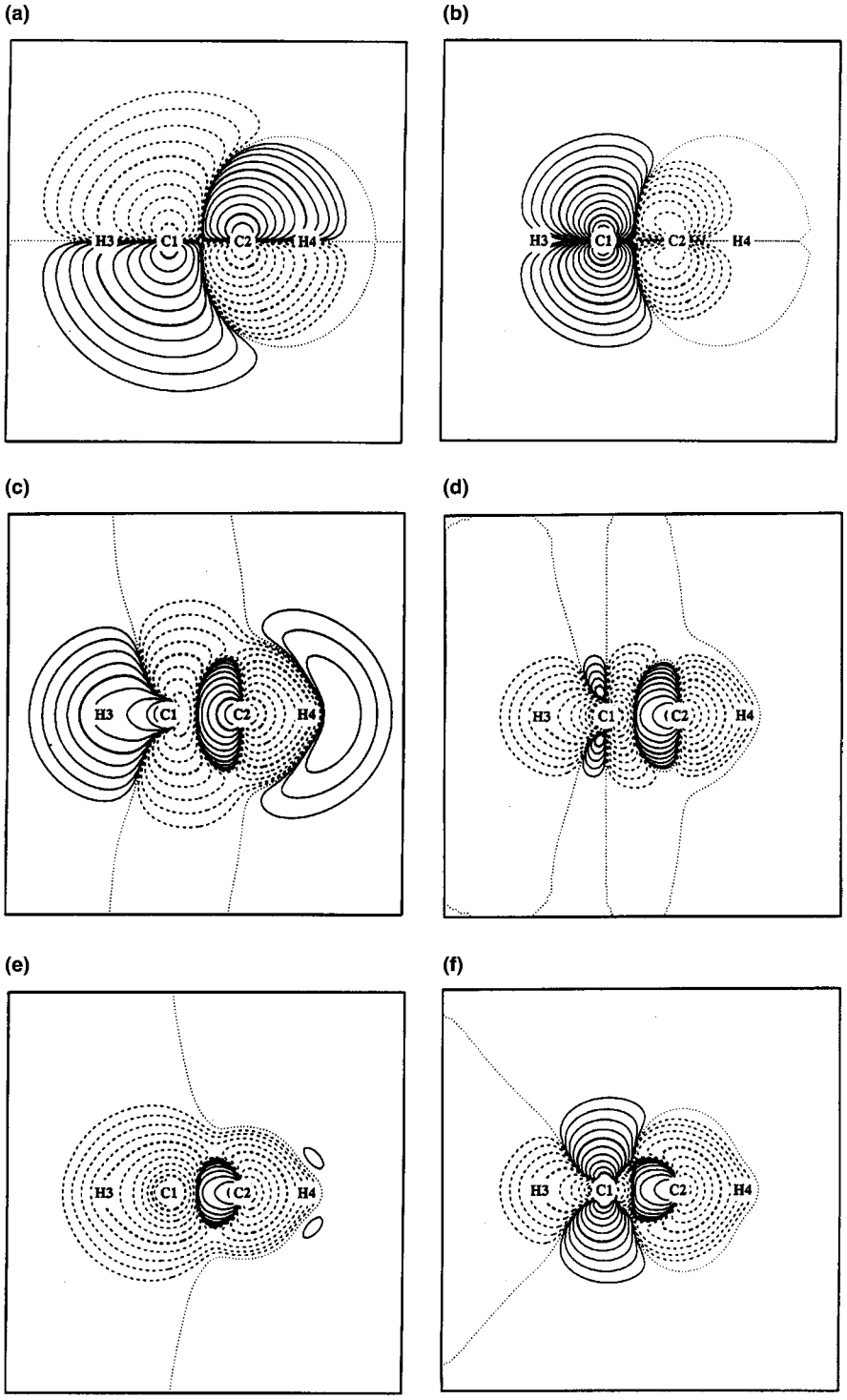

Fig. 2. Contour line diagrams of the current densities induced by the PSO coupling mechanism and the PSO density distribution for C_2H_2 in a plane containing the molecular axis. All calculations done at the BPW91/ (11s, 7p, 2d/6s, 2p)[7s, 6p, 2d/4s, 2p] level of theory using the experimental geometry [23]. The contour levels are chosen equally tempered, i.e., in a geometric progression. The bold lines denote contour levels of 0.1 and 10; the relative spacing between two adjacent contours is $100^{1/5} = 2.5118864$. Solid lines denote positive, dashed lines negative and the dotted lines a zero value of the current density (or the PSO density). In the current density diagrams, positive (negative) values indicate a current out of (into) the drawing plane. The perturbing nuclear moment is at C2: (a) current density in the *yz*-plane for the perturbing moment parallel to the C≡C axis (*z*-direction); (b) PSO density in the *yz*-plane for the perturbing moment parallel to the C≡C axis (*z*-direction); (c) current density in the *yz*-plane for the perturbing moment perpendicular to the C≡C axis in *y*-direction; (d) PSO density in the *yz*-plane for the perturbing moment perpendicular to the C≡C axis in *y*-direction; (e) PSO density in the *yz*-plane for the perturbing moment perpendicular to the C≡C axis in *x*-direction; (f) PSO density averaged over all orientations of the perturbing moment.

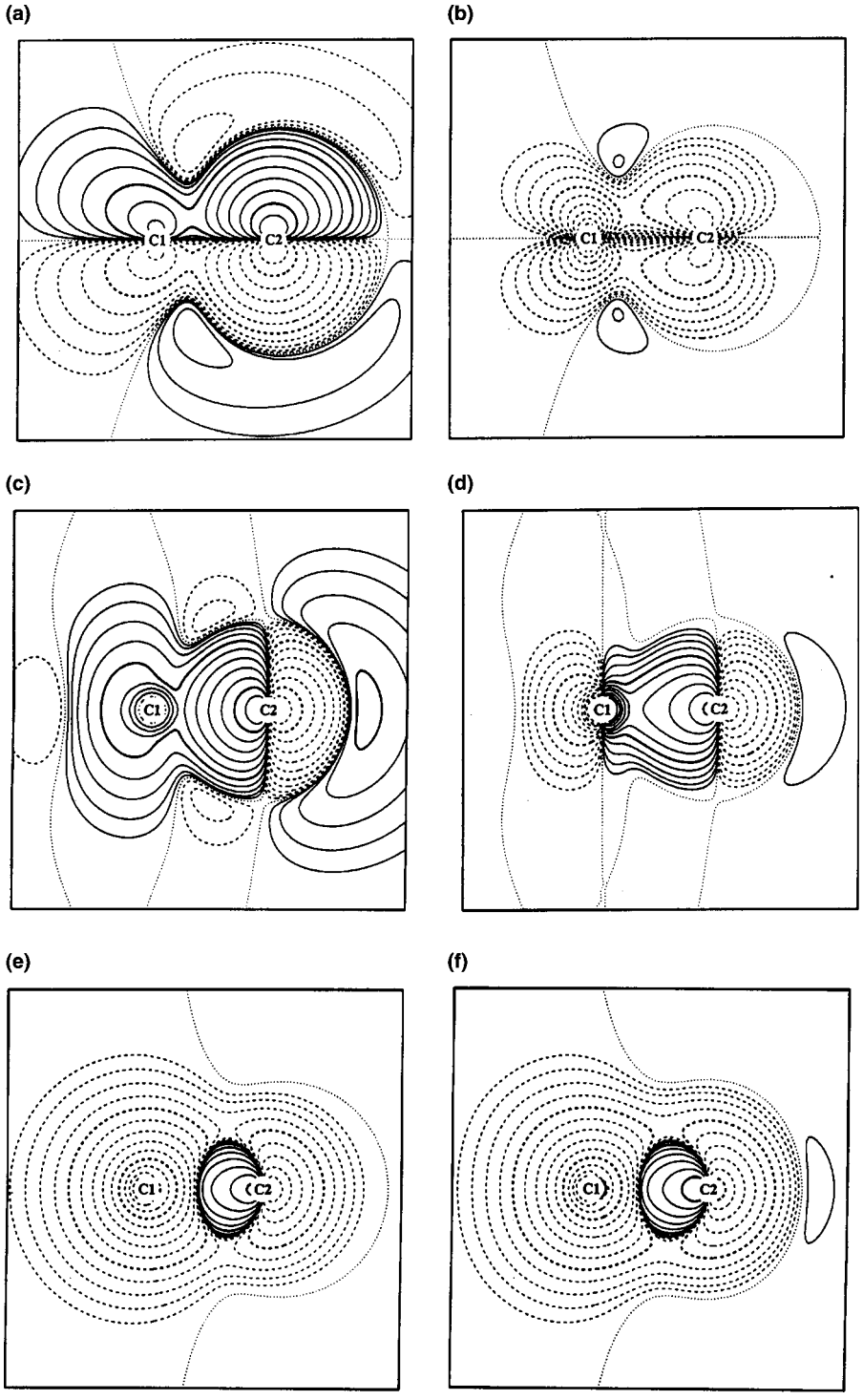

Fig. 3. Contour line diagrams of the current densities induced by the PSO coupling mechanism and the PSO density distribution for C_2H_2 in the *yz*-plane containing the C═C bond and orthogonal to the molecular plane (*xz*-plane). All calculations done at the BPW91/ (11s, 7p, 2d/6s, 2p) [7s, 6p, 2d/4s, 2p] level of theory at the experimental geometry [24]. For further details, see caption of Fig. 2: (a) current density for the perturbing moment parallel to the C═C axis (*z*-direction); (b) PSO density for the perturbing moment parallel to the C═C axis (*z*-direction); (c) current density for the perturbing moment perpendicular to the C═C axis in *y*-direction; (d) PSO density for the perturbing moment perpendicular to the C═C axis in *y*-direction; (e) PSO density for the perturbing moment perpendicular to the C═C axis in *x*-direction; (f) PSO density averaged over all orientations of the perturbing moment.

plane of the $\pi^*_{\pm}$ orbitals, which is in the plane bisecting the C≡C bond and standing perpendicular to it, ensures that the local contributions to $\langle \pi^*_{\pm} | h_z^{(C2),PSO} | \pi_{\pm} \rangle$ from the region around C2 (where the magnetic field **B** points to the right, Fig. 1c) and around C1 (where **B** points to the left) have the same sign (the vector product in Eq. (10)

becomes positive in both cases) and add up. Circumstances (i), (ii) and (iii) account for the resulting large ring currents. Regarding the weighting of the current density, it is known from magnetostatics (Biot–Savart law) that the magnetic field of a ring current decays with the 3rd power of the distance from the ring axis. This explains why the ring currents around Cl are much more effective (larger PSO densities close to the nucleus; Fig. 2b) than those around C2 for the PSO term. Accordingly, a large positive value of $^1K_{zz}^{\mathrm{PSO}}$(CC) (63.3 SI units, Table 2) results. This value is exactly twice the contribution of each π(CC) orbital (see Table 2), which reflects the fact that all other orbitals have σ character and thus do not contribute to PSO_{zz}.

Fig. 2c presents the current density for C_2H_2 in the *yz*-plane with the perturbing nuclear moment in *y* direction, i.e., perpendicular to the C≡C bond axis in the drawing plane. The contour plot shows two ring currents, with equal orientation, one around C2 and one around an axis close to C1. The corresponding PSO density is shown in Fig. 2d. In the region around C2, the PSO density looks similar to the current density itself. One sees that the ring current around C2 makes both positive and negative contributions to the PSO term, which partially cancel each other. Around C1, however, the orientation of the weight factor gives rise to an additional nodal plane. As a consequence, the sign of the PSO density is uniformly negative around C1, except for a small (perpendicular) ring close to C1. These negative contributions eventually give rise to a value of −18.0 SI units calculated for $^1K_{yy}^{\mathrm{PSO}}$(CC) (Table 2). An orbital analysis shows that a large part of the ring currents is carried by excitations (i) from the σ_z(CC) orbital into the appropriate π^*(CC) orbital and (ii) from π_x(CC) orbital into the σ_z^*(CC) orbital. Both excitations give rise to a pair of equally oriented ring currents as it is observed in Fig. 2c. The resulting orbital contributions are −13.0 SI units for the σ_z(CC) and 1.2 SI units for the π_x(CC) orbital.

The perturbing moments in *x* and *y* direction are symmetry-equivalent for C_2H_2 and, therefore, there is no need to repeat the analysis for the *x*-direction. As a matter of fact, the current density in the *xy*-plane bisecting the C≡C bond vanishes because of opposite current directions in this plane. Instead, it is interesting to consider the PSO density resulting from the in-plane currents (*yz*-plane), which is symmetry-equivalent to the PSO density in the *xz*-plane resulting from a perturbation in *y* direction. This PSO density is shown in Fig. 2e. One finds again a dominance of negative contributions and a region with positive contribution left to C2.

The orientation-averaged PSO density for C_2H_2 is shown in Fig. 2f, which gives a superposition of the features discussed for Figs. 2b, d and e. The toroidal region with positive contributions around C1 from the *zz* term still dominates, but is partly compensated by the negative contributions arising from the *xx* and *yy* terms. The contributions from the ring currents in *x* and *y* direction are averaged cylindrical around the axis of the molecule. Hence, the integral over the total PSO density (see Eq. (10)) is smaller than the large positive $^1K_{zz}^{\mathrm{PSO}}$ (CC) value leading to an isotropic PSO value of just 9.1 SI units (Table 2).

3.2. The PSO term for ^1J(CC) of ethylene

In the case of ethylene, there is no pair of degenerate π orbitals in C_2H_4 and therefore we use real π orbitals in the following discussion. Fig. 3a shows the perpendicular ring current density for C_2H_4 for the perturbing moment parallel to the C=C bond. Note that the π_y (C=C) orbital is intersected by the drawing plane (*yz*-plane). The ring currents are considerably weaker than for C_2H_2 (Fig. 2a), which becomes obvious when following the outermost bold contour line from C2 to C1 (Fig. 3a). Besides, the ring current is oriented uniformly throughout the molecule, the current around C2 being larger than that around C1. The PSO density is shown in Fig. 3b. It is predominantly negative, leading to a value of −5.4 SI units for $^1K_{zz}^{\mathrm{PSO}}$ (CC) (see Table 2).

For excitations from the π_y orbitals, there are no virtual π orbitals available but only pseudo-π orbitals, i.e., orbitals composed of a 2pπ(C) orbital and an antisymmetric combination of the 1s orbitals at the neighboring H atoms. The lowest of these virtual orbitals is the pseudo-$\pi_x^*(H_2CCH_2)$ orbital, which overlaps only moderately with the π_y orbital. Apart from this, it is C–C bonding, i.e., the local contributions to $\langle$pseudo-$\pi_x^*|h_z^{(\mathrm{C2}),\mathrm{PSO}}|\pi_y\rangle$ from the regions around C2 and around C1 cancel each other partly thus leading to a smaller current density at C1 (Fig. 3a). Finally, its energy relative to the HOMO (BPW91/[7s,6p,2d/4s,2p] orbital energies: −0.246 and +0.064 a.u., respectively), is higher than for the $\pi_\pm \rightarrow \pi_\pm^*$ excitations in C_2H_2. These circumstances account for the lower efficiency of the induction mechanism as compared to C_2H_2. The perturbing field is strongest around C2 and the orientation of the ring current is determined by the field in this region. Consequently, the contribution of the ring current to the PSO term is negative. Its value is just −0.7 SI units, or about 14% of the total $^1K_{zz}^{\mathrm{PSO}}$ (CC) value (Table 2). The remaining part of the PSO_{zz} term is due to excitations from the σ(CH) bonds into the π_x^*(CC) orbital.

Clearly, the π_y (C=C) orbital is much less effective for the induction of ring currents around the C=C axis than the π system in C_2H_2. The in-plane pseudo-π_x (H_2CCH_2) and pseudo-$\pi_x^*(H_2CCH_2)$ orbitals can only insufficiently play the role of the $\pi_\pm$ and $\pi_\pm^*$ orbital of acetylene and therefore the conducting cylinder around the CC axis found for acetylene is strongly distorted in the case of the ethylene molecule. Most important is the

CC bonding character of the pseudo-$\pi_x^*(H_2CCH_2)$ orbital contrary to the antibonding character of the $\pi_\pm^*$ orbital in acetylene. Note that the $\pi_y \rightarrow \pi_y^*$ excitation cannot contribute to the PSO mechanism since the PSO operator is an angular momentum operator.

The current density distribution in the *yz*-plane for the perturbation in the *y* direction is shown in Fig. 3c. There is a ring current around C2, but contrary to acetylene (Fig. 2c) there is no second ring current around C1. The PSO density shown in Fig. 3d has a nodal plane through each C atom. Consequently, positive and negative contributions to the PSO term cancel each other to a large extent, thus leading to the relatively small value of −0.15 SI units for $^1K_{yy}^{PSO}$ (CC).

For the perturbation oriented in *y* direction, the main contribution to the ring current comes from the σ_z(CC) orbital and involves the excitation σ_z(CC) → pseudo-$\pi_x^*(H_2CCH_2)$. (The excitation pseudo-$\pi_x^*(H_2CCH_2) \rightarrow \sigma^*$(CC) plays a smaller role because of the high energy of the σ_z^*(CC) orbital.) These orbitals do not possess a nodal surface perpendicular to the bond axis, which implies that there are not two ring currents but just one around C2 while the perpendicular current density around C1 is uniformly positive (Fig. 3c) as already discussed in connection with the perturbation in the *z*-direction (Fig. 3a). Neither the ring current around C2 nor the uniform current around C1 generates a sizable magnetic field at C1, which explains the small value of the *yy* component of the PSO term. The orbital analys reveals that the contribution of the σ_z(CC) orbital to PSO_{yy} is −2.0 SI units, i.e., much larger than the total PSO_{yy} value. Actually, contributions from the σ(CH) orbitals compensate a large part of the σ_z(CC) contribution.

Fig. 3c shows that the paramagnetic current may violate the continuity equation: There is a clear overweight of the out-of-plane current, which will be compensated by a surplus of the in-plane DSO current density. This underlines the fact that the splitting of the spin–orbital part of the SSCC into PSO and DSO contribution is connected with some arbitrariness and only done to facilitate the analysis of PSO and DSO term.

For the perturbing moment oriented in *x* direction, the induced currents are in the molecular plane (*xz*-plane). As in the case of acetylene, the current density vanishes in the *xy*-plane bisecting the C═C bond. The current density in the *yz*-plane (not shown) resembles that displayed for C_2H_2 in Fig. 2c as is confirmed by the PSO density (Fig. 3e) shown for the *yz*-plane. Indeed, an orbital analysis shows that the main contribution arises from the excitation $\sigma_z(CC) \rightarrow \pi_y^*$, which gives rise to a pair of ring currents around C1 and C2. The resulting value for $^1K_{xx}^{PSO}$ (CC) is −33.8 SI units, which is of the same order of magnitude than the corresponding value for C_2H_2 (−18.0 SI units, Table 2). The larger value for ethylene is due to the stronger p_z character of the σ_z(CC) orbital in ethylene (sp^2 rather than sp) and to the fact that, because of the larger electronegativity of a sp-hybridized C atom, the σ_z and π orbital are lower and the π^* higher in energy than in ethylene. Consequently, the excitation energy $\sigma_z(CC) \rightarrow \pi_y^*$ in ethylene is significantly smaller thus leading to the larger magnitude of the PSO_{xx} contribution. The orientation-averaged PSO density shown in Fig. 3f resembles that for the perturbing moment oriented into *x*-direction (Fig. 3e). This is in line with the fact that the *xx* component of the PSO tensor dominates the isotropic average (see Table 2). The orbital analysis reveals that the σ_z(CC) orbital stands for the main contribution to PSO_{xx} (−18.0 SI units), while the second sizeable contribution comes from the π_y(CC) orbital (−7.1 SI units).

4. Chemical relevance of results

In this work, the principally different PSO contributions obtained for the SSCC $^1K(CC)$ (or $^1J(CC)$) of double and triple bonds are explained. The analysis reveals that the isotropic PSO term is a consequence of several, sometimes contradicting factors: (a) the existence of orbital pairs (occupied, virtual) with pπ character and the right angular relationship, i.e., *xy*, *xz* or *yz* for perturbation in the *z*, *y* or *x* direction. The second component of the orbital pair is important for the nodal behavior of the first order orbital; (b) the induction of strong ring currents requires low excitation energies from the *x* to the *y* (*y* to *x*), the *x* to the *z* (*z* to *x*) or *y* to the *z* (*z* to *y*) component of the orbital pairs; (c) the orbital overlap between zeroth order and the first order orbital influence the magnitude of the ring current where one has to consider that two terms enter Eq. (11) as the gradient of the orbital can be taken with regard to the zeroth or first order orbital; (d) the nodal properties of zeroth and first order orbital are decisive whether a local ring current is increased or decreased. The direction of the nuclear dipole field in combination with the nodal properties of the orbitals involved decides on the direction of the local ring currents; (e) the weighting factor of Eq. (10) can lead to the introduction of additional nodal surfaces into the PSO density. The PSO densities shown in this work reveal that with an increase of the number of nodal surfaces in the PSO density the magnitude of the corresponding PSO component decreases.

On the basis of these general observations one can rationalize the PSO components for the SSCC of ^1K(CC) in staggered ethane (Table 2). Suitable orbital pairs are (pseudo-π_x, pseudo-π_y^*) for the *z*-perturbation, (pseudo-π_x, σ_z^*) for the *y*-direction and (pseudo-π_y, σ_z^*) for the *x*-direction. The excitation energies are relatively large so that the ring currents will be rather weak. As in the case of acetylene, there should be two components of the same magnitude and sign, i.e., $PSO_{yy} = PSO_{xx}$ and a

third component (PSO_{zz}) with different magnitude and sign. Since the pseudo-$\pi(H_3C–CH_3)$ orbitals have a different nodal behavior in the CC bond than the π orbitals in acetylene (pseudo-π has a nodal surface perpendicular to the CC axis bisecting the latter, pseudo-π^* does not have such a nodal plane), the signs of the PSO components should be opposite to the corresponding PSO components of acetylene. The magnitude of the PSO_{zz} component should be larger than those of the other components for the same reasons as discussed for acetylene. Since the excitation energies imply in general much smaller values, there is not a similar dominance of PSO_{zz} as in the case of acetylene. Accordingly, the three PSO components will cancel each other largely in the isotropic average yielding a relatively small PSO contribution for ^1K(CC) in ethane. These predictions are confirmed for the PSO contributions listed in Tables 1 and 2. The PSO term has a value of just −0.03 SI units, which however does not mean that there are no orbital currents in ethane, only that positive and negative PSO components cancel each other largely. This will hold for all single bonds similar to the ethane single bond, however it can change as soon as the CC single bond is strained (getting more p-character) as in small ring molecules.

The PSO term reflects the electronic structure of a molecule in a more complex way than the FC term does. It reflects the existence of pairs of pπ molecular orbitals such as (π_x, π_y^*) (pseudo-π_x, π_y^*) (pseudo-π_x, pseudo-π_y^*), (π_x, σ_z^*), (pseudo-π_x, σ_z^*), (π_y, σ_z^*), etc., which are responsible for ring currents around the bond axis (z-perturbation) or for the ring currents around the two axes perpendicular to the bond axis (x- and y-perturbation). The magnitude of the resulting PSO component is a direct reflection of the magnitude of the lowest excitation energy because the corresponding orbital term should dominate the PSO component. Thus, the $\pi_x \rightarrow \pi_y^*$ excitation energy is smaller than the pseudo-$\pi_x \rightarrow \pi_y^*$ excitation energy, which in turn is smaller than the pseudo-$\pi_x \rightarrow$ pseudo-π_y^* excitation energy. The corresponding PSO_{zz} components decrease in magnitude from 63 to $|-5.4|$ and $|-2.0|$ SI units (see Table 2). Similar relationships hold for excitations involving the σ_z orbital.

Decisive for the PSO term is actually the density. If this density is distorted by environmental effects such as the presence of a second molecule in a complex, the PSO term can increase in magnitude even if the bond in question is formally considered to involve just s-electrons. The correct description of the distortion of the density implies the admixture of p-type functions, which enter the formulas for the PSO components given in this work.

Since the sign of the different PSO components mostly differ, a sizable isotropic PSO value will be only obtained if one of the PSO components dominates largely: this is for triple bonds the large positive PSO_{zz} value caused by the cylindric ring currents around the bond axis. For double bonds, the π_y or π_y^* orbital must be involved, which indicates that the largest contribution is PSO_{xx}.

We have shown in previous work that the Fermi contact spin density distribution at the nuclei depends on the electronegativity of the coupling atoms and the polarizability of atom (and bond) densities. The larger the polarizability is the better can spin polarization be transferred from one nucleus to the other. It can happen that electronegativity and polarizability effects are counteractive leading to a decrease in the magnitude of the FC term [17]. The electronegativity plays an important role also for the PSO term, however in a more indirect way. Since the C atom in ethylene (less s-character) has a lower electronegativity than a C atom in acetylene (more s-character), the energies of relevant occupied orbitals are higher, those of relevant virtual orbitals are lower thus leading to smaller excitation energies and a larger impact of the corresponding PSO component. The role that is played by the polarizability in the case of the FC term is taken over by the magnetizability ξ. It is well known that the ξ-increment for the CC triple bond is 232×10^{-30} J T $^{-2}$ while that for a double bond is just -58×10^{-30} J T $^{-2}$ [26].

Another factor beside electronegativity and magnetizability is the topology of π-bonding. Formal single bonds between π-bonds should be associated with a significant PSO contribution to the corresponding one-bond SSCC larger than that of ethane. At the same time, the highest occupied π orbital has a nodal plane cutting through the formal single bond so that the corresponding PSO density will have, contrary to that of an isolated double bond, also a nodal surface. Areas with positive and negative density will cancel so that the PSO term for the corresponding one bond SSCC will be probably closer to that of a single bond than its π-bond character suggests. Nevertheless we predict that the PSO term will be (together with the SD term) a useful descriptor for the determination of the π-character of a bond. Following the procedure described in the introduction it should be possible to use measured SSCCs, derive the FC term in another way and determine the NC terms as the difference between these quantities. Work is in progress to explore this possibility of describing the π-character of bonds.

Acknowledgements

This work was supported by the Swedish Research Council (Vetenskapsrådet). J.G. thanks Carl Tryggers Stiftelse for financial support. Calculations were done on the supercomputers of the Nationellt Superdatorcentrum

(NSC), Linköping, Sweden. We thank the NSC for a generous allotment of computer time.

References

[1] See D.M. Grant, R.K. Harris (Eds.), Encyclopedia of Nuclear Magnetic Resonance, vols. 1–8, Wiley, Chichester, 1996.
[2] J.A. Pople, W.G. Schneider, H.J. Bernstein, High-resolution Nuclear Magnetyic Resonance, McGraw-Hill, New York, 1959.
[3] J.W. Emsley, J. Feeney, L.H. Sutcliffe, High-resolution Nuclear Magnetic Resonance Spectroscopy, Pergamon, Oxford, 1966.
[4] N.F. Ramsey, Phys. Rev. 91 (1953) 303.
[5] K. Jaakko, P. Lantto, J. Vaara, J. Jokisaari, J. Am. Chem. Soc. 120 (1998) 3993.
[6] T.A. Ruden, O.B. Lutnaes, T. Helgaker, J. Chem. Phys. 118 (2003) 9572.
[7] H.-O. Kalinowski, S. Berger, S. Braun, ^{13}C-NMR-Spektroskopie, Georg Thieme Verlag, Stuttgart, 1984.
[8] S. Berger, S. Braun, H.-O. Kalinowski, NMR Spectroscopy of the Non-metallic Elements, Wiley, Chichester, 1997.
[9] N. Muller, D.E. Pritchard, J. Chem. Phys. 31 (1959) 768.
[10] W.A. Bingel, W. Lüttke, Angew. Chem. 93 (1981) 944; Angew. Chem. Int. Ed. Engl. 20 (1981) 899.
[11] K. Frei, H.J. Bernstein, J. Chem. Phys. 38 (1963) 1216.
[12] V. Sychrovsky, J. Gräfenstein, D. Cremer, J. Chem. Phys. 113 (2000) 3530.
[13] A. Wu, D. Cremer, A.A. Auer, J. Gauss, J. Phys. Chem. A 106 (2002) 657.
[14] A. Wu, D. Cremer, J. Phys. Chem. A 107 (2003) 1797.
[15] J. Gräfenstein, A. Wu, D. Cremer, J. Am. Chem. Soc. (submitted).
[16] A. Wu, D. Cremer, Phys. Chem. Chem. Phys. 5 (2003) 4541.
[17] A. Wu, J. Gräfenstein, D. Cremer, J. Phys. Chem. A 107 (2003) 7043.
[18] A.D. Becke, Phys. Rev. A 38 (1988) 3098.
[19] J.P. Perdew, in: P. Ziesche, H. Eschrig (Eds.), Electronic Structure of Solids '91, Akademie-Verlag, Berlin, 1991, p. 11.
[20] J.P. Perdew, Y. Wang, Phys. Rev. B 45 (1992) 13244.
[21] W. Kutzelnigg, U. Fleischer, M. Schindler, in: NMR – Basic Principles and Progress, vol. 23, Springer, Heidelberg, 1990, p. 165.
[22] S. Huzinaga, Approximate Atomic Wave Functions, University of Alberta, Edmonton, AB, Canada, 1971.
[23] A. Baldacci, S. Ghersetti, S.C. Hurlock, K.N. Rao, J. Mol. Spectrosc. 39 (1976) 116.
[24] H.C. Allena, E.K. Plyler, J. Am. Chem. Soc. 80 (1958) 2673.
[25] E. Kraka, J. Gräfenstein, M. Filatov, Y. He, J. Gauss, A. Wu, V. Polo, L. Olsson, Z. Konkoli, Z. He, D. Cremer, COLOGNE 2003, Göteborg University, Göteborg, 2003.
[26] W.H. Flygare, Chem. Rev. 74 (1974) 653.